Nat Hazards
DOI 10.1007/s11069-015-1788-5

ORIGINAL PAPER

Risk assessment of groundwater pollution with a new methodological framework: application of Dempster–Shafer theory and GIS

Aminreza Neshat[1] · **Biswajeet Pradhan**[1]

Received: 4 November 2014 / Accepted: 1 May 2015

Abstract Managing natural groundwater resources is challenged by nitrate pollution resulting from agricultural activities. This issue is emerging as an important environmental concern that needs to be addressed through effective groundwater management. Groundwater assessment is an important aspect of groundwater management, particularly in arid and semi-arid regions. This study focused on the Kerman Plain, which is exposed to intensive agricultural activities and land exploitation that result in intense land pollution. The effects of nitrate pollution may be controlled by applying specific measures. Dempster–Shafer theory (DST) was applied in this study to develop a new methodology for assessing pollution risk. Applying this theory as a pioneering approach to assessing groundwater pollution risk is the novel component of this research. This approach provides a major advantage by dealing with varying levels of precision related to information. The spatial association between DRASTIC parameters including D (depth of water), R (net recharge), A (aquifer media), S (soil media), T (topography), I (impact of vadose zone) and C (hydraulic conductivity) and underground nitrate occurrence was evaluated by applying bivariate DST to assign mass functions. Dempster's rule of combination using GIS was then applied to determine a series of combined mass functions for multiple hydrogeological data layers. The uncertainty of system responses was directly addressed by the proposed methodology. Finally, the modified DRASTIC map with the highest validity and accuracy was selected and combined with the damage map. The comparison between nitrate distribution and vulnerability and the risk maps exhibit high similarity between different vulnerability degrees and nitrate concentrations. Long-term planning of preventive measures and associated developments can be aided by the regions with low and very low risks located in the northeast, northwest, and central regions.

✉ Aminreza Neshat
neshat.aminreza@gmail.com

✉ Biswajeet Pradhan
biswajeet24@gmail.com

[1] Department of Civil Engineering, Faculty of Engineering, Geospatial Information Science Research Center (GISRC), University Putra Malaysia, 43400 Serdang, Selangor, Malaysia

Published online: 15 May 2015

Keywords Dempster–Shafer theory · GIS · Nitrate · Risk assessment · Hydrogeological parameters

1 Introduction

A significant environmental concern is associated with risk assessment and management of water quality. Government regulations and scientific investigations are focused on these environmental concerns, thus implying that human health and other associated activities are under constant threat from groundwater pollution. Further attentions should be given to issues related to the groundwater pollution because such issues are diverse and complicated, affecting groundwater quality in different ways.

In particular, arid and semi-arid regions are dependent on groundwater as a major water source (Neshat and Pradhan 2014). Methods for cleaning and restoring contaminated water to its natural quality are typically costly and complicated. In many cases, an alternative water source is not an option in terms of feasibility. Therefore, protecting groundwater from pollutants is a viable solution.

The probability of pollutants seeping through the ground and reaching groundwater sources is determined through groundwater vulnerability assessment reports. The paths followed by nutrients reaching surface water are also reflected in groundwater. Thus, surface water can pose an ecological threat in the form of excess nitrogen (Tesoriero et al. 2009). Surface water does not contain nitrates. The movement of contaminants from surface water to groundwater can be sufficiently indicated by nitrate, which is particularly useful in agricultural areas (Javadi et al. 2011; Neshat et al. 2013). Variable of concentrations on nitrate may be found in groundwater. According to recent studies, nitrate concentration in drinking water can increase to dangerous levels, even when nitrate ingestion is below the WHO guideline of 50 mg/L.

The occurrence of groundwater pollution can be expressed as a probability of the spatial occurrence of nitrate concentration over a set of hydrogeological factors that use the statistical properties of measured points for interpolation, that is, geostatistical interpolation technique (e.g., kriging). A predicted value for an unmeasured location can be derived from ordinary kriging (OK) technique by weighting the surrounding measured values. The spatial autocorrelation of measured points is quantified via the geostatistical technique. OK is also among the most common interpolating methods in agriculture practices (Mishra et al. 2010).

The concepts of lower and upper probabilities found in multi-valued mapping were proposed by Dempster (1967). Shafer (1976) further elaborated on the concept and extended it to current D–S theory of evidence. A range is used to present probabilities in DST. This range includes belief (Bel) and plausibility (Pls) functions, wherein the smallest probability is represented by the Bel function based on available evidence, whereas the highest probability is denoted by the Pls function. The sum of the Bel function and the uncertainty is called the Pls function. Therefore, DST is a more generalized form of probability theory. DST is also flexible when accepting uncertainties and can combine beliefs extracted from multiple sources of evidence, which is a major advantage of this approach (Thiam 2005).

Various uncertainties may plague assessment because of incomplete, inaccurate, and contradictory data related to groundwater pollution. Such uncertainties should be formulated in a geographic information system by categorizing them (Malpica et al. 2007). The DST can be used for assessing risk under uncertainty. As such, uncertainties associated with single-point probabilities are captured in this approach (Chowdhury et al. 2009).

2 Previous works

Groundwater significance was assessed at a global scale in light of expanding industrial and agricultural activities. This topic has attracted many researchers (Cucchi et al. 2008; Manos et al. 2010; Sorichetta et al. 2011; Anane et al. 2012; Fijani et al. 2013; Pacheco and Fernades 2013; Pavlis and Cummins 2014; Neshat et al. 2014).

Information related to whether the concentration of a specific contaminant was more than the threshold value was extracted from the isoprobability map (Assaf and Saadeh 2009; Chen et al. 2013). Baalousha (2010) applied the DRASTIC approach to preparing a vulnerability map for a study area. Kriging variance was then used to verify the spatial distribution of the sites. Geostatistical techniques, such as indicator kriging (IK) and ordinary kriging (OK), have been used by researchers to execute various applications such as creating isoconcentration maps of groundwater contaminants (Stigter et al. 2006). There are various forms of kriging: ordinary kriging, simple kriging, universal kriging, and cokriging as well as residual kriging (Bayat et al. 2014). The probability that groundwater resources might be polluted by contaminants which are introduced into the ground surface is expressed as specific vulnerability or pollution risk. This is revealed by the groundwater intrinsic vulnerability and the contaminant loading which is employed to the specific point of the hydrogeological region. The contaminant loadings are defined by extent, the physicochemical features and the procedure of different contaminants of distribution in an area. The COP methodology was applied by Dimitriou et al. (2008) in vulnerability and risk mapping, along with the European Cooperation in Science and Technology Action 620, which is a project of the European Union. The information obtained has been indicated in various studies on groundwater pollution risk assessment. The objective of protecting carbonate aquifers was achieved through the aforementioned mapping. The DRASTIC model was used by Leone et al. (2009) to assess the risks and vulnerability of agricultural potential and nitrogen pollution. The degree of risk that affects the study area was determined by Saidi et al. (2011) by combining the hydrogeological parameters of the DRASTIC method and hazard assessment. Risk mapping was assessed by Wang et al. (2012) by applying a combination of intrinsic vulnerability, groundwater values, and hazards. A specific groundwater vulnerability in central Florida was created by Van Beynen et al. (2012), using a new GIS-based index, the Karst Aquifer Vulnerability Index (KAVI), integrates geologic layers applied in intrinsic groundwater vulnerability models (GVMs) and over an epikarst layer specific to karst with land use coverage. A probability-based DRASTIC model of aquifer vulnerability was used by Chen et al. (2013) on the Choushui River alluvial fan. The evaluated vulnerability index was used to ascertain various risk categories of contaminants. The nitrate pollution categorical map was further expanded by applying a methodology based on nonparametric and nonlinear methods of indicator kriging (Chica–Olmo et al. 2014). Monte Carlo Simulation was also performed for groundwater pollution risk estimation in an agriculture region (Neshat et al. 2015).

Various topics used DST in the environmental sector. Mineral potential mapping has been conducted through this model in knowledge-based approaches (Moon 1990; An et al. 1992). DST was also used in the data-driven mineral potential mapping method of Carrazan and Hale (2002). The data-driven DST model has been successfully applied in many

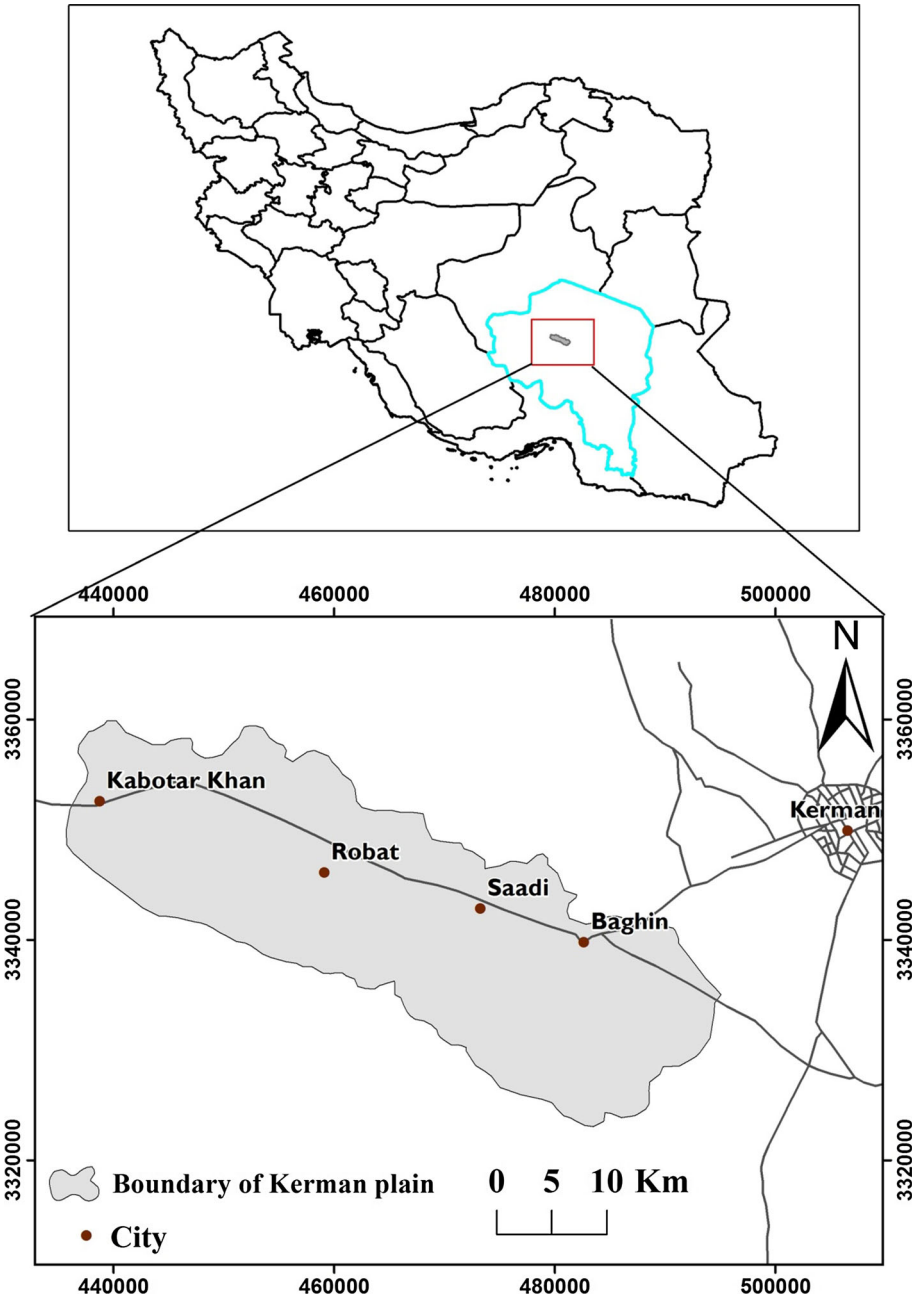

Fig. 1 Location of study area

studies, such as mineral potential mapping (Carranza 2011; Carranza and Sadeghi 2010), pre-eruption prediction of lahar-inundation zones (Carranza and Castro 2006), geothermal potential mapping (Carranza et al. 2008), groundwater potential mapping (Nampak et al. 2014), and land subsidence susceptibility (Pradhan et al. 2014). Ghosh and Carranza (2010) used the data-driven DST model to map rockslide-prone areas located in Darjeeling Himalaya (India). Land-cover estimation and monitoring techniques have also been defined in various studies (Cayuela et al. 2006). Successful implementation of landslide susceptibility mapping has also been observed in several studies (Mohammady et al. 2012; Tien Bui et al. 2012, 2013; Feizizadeh and Blaschke 2012; Jebur et al. 2015).

In the present study, DST was chosen as a novel approach to assessing groundwater pollution risk in Kerman Plain, Iran. This study focused on the southeast part of Iran, given that surface water scarcity in this area made groundwater as the primary source. Agricultural regions constitute most of the study area, and such regions are frequently exposed to fertilizers.

This paper is organized as follows: First, the best validation result for groundwater vulnerability (modified DRASTIC) in the Kerman Plain was selected. Interpolation of the last nitrate samples (May 2012) was then executed by applying ordinary kriging (OK). Maximum probability was determined by considering the uncertainty from nitrate. Finally, the groundwater pollution risk map was produced.

3 Study area and data

An arid/semi-arid region located in the Kerman Plain was selected for this study (Fig. 1). The study area is approximately 978 km^2 and lies in the southeastern part of Iran. The altitude of this region ranges from 1633 m to 1980 m above sea level. In 2011, the average annual rainfall in the area amounted to 108.3 mm. A hot and dry summer is prevalent in this region, along with a relatively rainy winter as well as a short spring and autumn. At least 2 months, typically January and February, are glacially related within a typical water year. However, according to water organizations in Kerman, this phenomenon has decreased in recent years because of climate change. Groundwater is an essential water source for cultivating pistachio, which is a primary agricultural product that supports the economy of Kerman Plain.

According to a geological survey of Iran, Cretaceous and Eocene conglomerates, intrusive rocks, Eocene and Neogene volcanism products, and Neogene or younger sediments constitute the geology of Kerman Plain. Marl and conglomerate rocks in the south and in a small region in the northwest are the main materials that constitute the aquifer media. The regions across the north and the northeast are based on fine–medium sand. Silt and clay deposits constitute the central regions. Sand deposits with an extremely low fine-grained material ratio, called gravel and sand, are found in considerable quantity. A mixture of gravel, sand, silt, and clay represents the glacial till, which was introduced by Aller et al. (1987). This study deals mostly with clay loam, gravel, non-shrinking loam, non-aggregated clay, sandy loam, and silty loam in the study area. In the north and south sections of the study area, sand with high permeability is investigated as the available soil media layer.

This study deals with depths ranging from 15 m to more than 30 m in the Kerman Plain. Three categories of depths are used, namely, 15–23 m, 23–30 m, and >30 m. The third category is frequently formed the study area. Irrigation return flow is denoted by two classes that are less than 30 m, provided that the study area is located in arid and semi-arid

regions. The main groundwater recharge sources in the area are based on rainfall infiltration, irrigation return flow, and absorption wells. Approximately 186.06 million cubic meters per year of total recharge is estimated in the study area (Neshat et al. 2014).

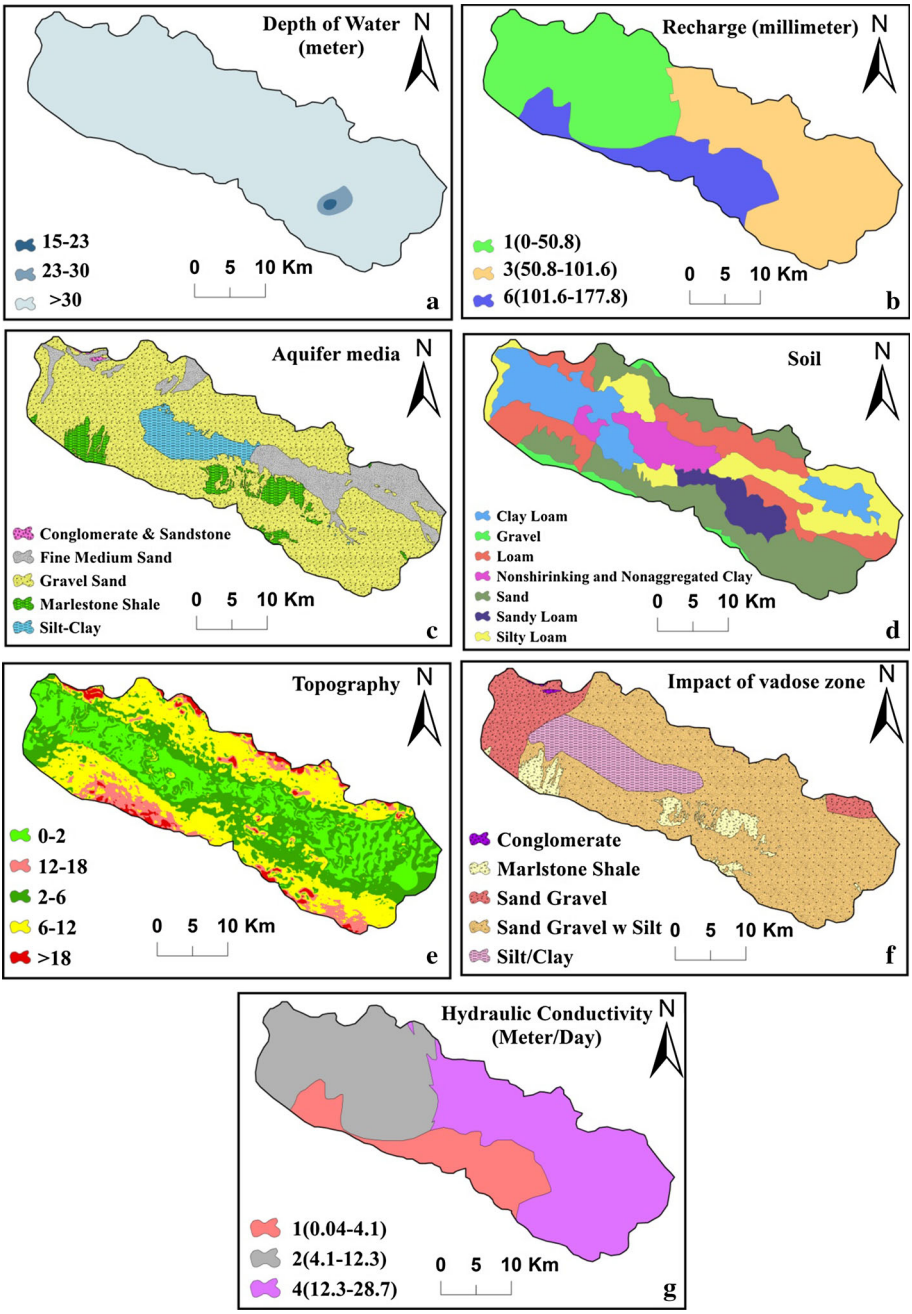

Fig. 2 Hydrogeological parameters of the Kerman plain

A topographic map is used to extract the topography from a digital elevation model (1:25,000). Slopes vary from 0 % to more than 18 %. Silt clay and sand gravel are found in the vadose zone in the western regions, whereas gravel and sand are located in a small region in the northeast. The study area displays a maximum conductivity of 3880 μmoh/cm, whereas the average of electrical conductivity (EC) is 2700 μmoh/cm and the minimum EC is approximately 1100 μmoh/cm. The maximum EC is exhibited in the southeast region of the study area.

4 Methodology

4.1 Groundwater vulnerability mapping

Aquifer characteristics, geology, and hydrogeology define the properties of groundwater vulnerability, which is a relatively dimensionless property. To create an effective monitoring network for groundwater resource management, groundwater vulnerability has an important role in defining the critical zones of an aquifer. Figure 2 illustrates the seven layers of DRASTIC parameters. Groundwater assessment can be conducted through various methods (Pacheco and Fernandes 2013). The DRASTIC method is the most commonly used technique to analyze groundwater vulnerability (Antonakos and Lambrakis 2007).

The DRASTIC method was modified in this study to assess groundwater vulnerability (Neshat et al. 2013). The following statistical processes were used for modification.

1. The Wilcoxon rank-sum nonparametric statistical test (Wilcoxon 1945) was applied to revise the rating scale of each parameter through the nitrate samples obtained in May 2010.
2. Single-parameter sensitivity analysis (SPSA) was conducted to revise the weight factors (Napolitano and Fabbri 1996).
3. The modified DRASTIC map was validated through nitrate samples obtained in May 2011, and subsequently, in May 2012. Pearson's correlation factor was used in the modified DRASTIC map and the original DRASTIC map. Hence, the former exhibited higher accuracy than the latter, thus making the modified DRASTIC map the obvious choice for this study (Neshat et al. 2013).

SPSA offers useful information on the effect of weighting values allocated to each parameter and helps analysts judge the importance of subjectivity (Babiker et al. 2005). The following equation is the final combined linear equation used for modified DRASTIC:

$$\begin{aligned}\text{Modified DRASTIC} = & D_{(\text{Wicoxon})}D_{(\text{SPSA})} + R_{(\text{Wicoxon})}R_{(\text{SPSA})} + A_{(\text{Wicoxon})}A_{(\text{SPSA})} \\ & + S_{(\text{Wilcoxon})}S_{(\text{SPSA})} + T_{\text{Wilcoxon}}T_{(\text{SPSA})} + I_{(\text{Wilcoxon})}I_{(\text{SPSA})} \\ & + C_{(\text{Wilcoxon})}C_{(\text{SPSA})}.\end{aligned} \quad (1)$$

The SPSA was also applied to evaluate the impact of each DRASTIC parameter on groundwater vulnerability by comparing actual and theoretical weights applied in DRASTIC. The modified DRASTIC model exhibited the highest accuracy compared with various optimizations of the DRASTIC model in the study area.

Given that the information related to this section has already been discussed by Neshat et al. (2013), this paper did not include an in-depth explanation in this section. Figure 3 illustrates the modified DRASTIC map.

4.2 Pollution

The first contamination effect caused by intense agricultural activities and widespread use of fertilizers in this region was identified as nitrate concentration. Nitrate concentration enters the soil from the surface and seeps its way to groundwater. Ordinary kriging (OK) is widely used method, when an interpolation is purely according to sample data, which needs dense sample data for an accurate interpolation (Wang et al. 2013). A total of 27 agricultural wells were used for sampling and analysis.

The last nitrate sample was collected in May 2012 and was subjected to OK interpolation to obtain nitrate concentrations in all pixels for the area that would help acquire the pollution parameters to assess risk in the Kerman Plain. The kriging method provided results with minimum estimation error variance, because it performed good spatial estimation from the sampling points (Baalousha 2010). Actual measurements on the field are not required for the kriging variance of estimate, which is the best linear unbiased estimator available for evaluating an unknown field. The OK interpolation equation is as follows:

$$Z^*(x_0) = \sum_{i=1}^{n} n\lambda_i Z(x_i). \tag{2}$$

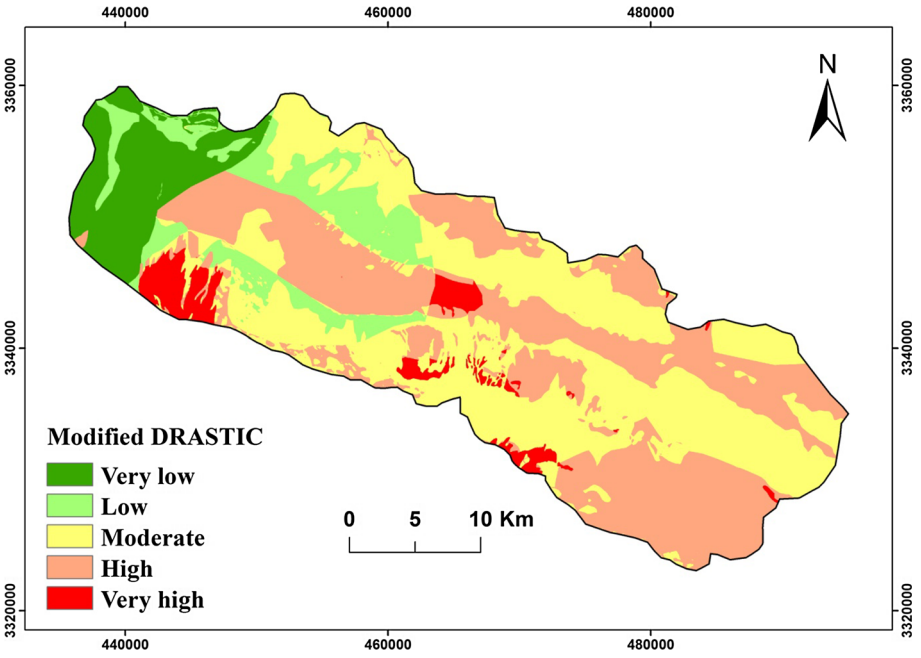

Fig. 3 Modified DRASTIC map

The estimated value is denoted by $Z^*(x_0)$, where n denotes the number of points. $Z(x_i)$ is the measured value at pointxi, and λ_i is the kriging weight.

The spatial distribution of nitrate concentration in the study area is shown in Fig. 4.

4.3 Dempster–Shafer theory (DST)

The belief (Bel) function was used in this study to present the probability by considering the uncertainties in the DRASTIC parameters of the nitrate concentration obtained in May 2012. Three relevant representations of belief were used in the Bel function framework: the Bel, the plausibility (Pls), and the basic probability assignment (m or bpa). Initial judgments are frequently explained through basic probability, whereas the final judgments on groundwater pollution risk are expressed through Pls.

The evidence is mathematically represented through DST. DST takes an alternative approach to estimating those probabilities. It evaluates the closeness of the evidence in proving the truth of the hypothesis, rather than the probability that the hypothesis is true.

The definitions of all possible hypotheses were used to initiate DST, which is denoted as Θ and called a frame of discernment. The sample space considered in the probability is equal to this value. A set of mutually exclusive and exhaustive propositions comprises the frame of discernment $\Theta = \{A_i, \quad i = 1, 2, 3, \ldots\}$.

The function m: $2^{\Theta} \rightarrow [0, 1]$ denotes the basic probability. The set of all subsets of A is denoted by 2^{Θ}, which also includes the empty set and 'A' itself.

Equation (3) is satisfied by this function, which is called the mass function, where $\emptyset$ is an empty set and A is any subset of Θ.

$$m(\emptyset) = 0 \tag{3}$$

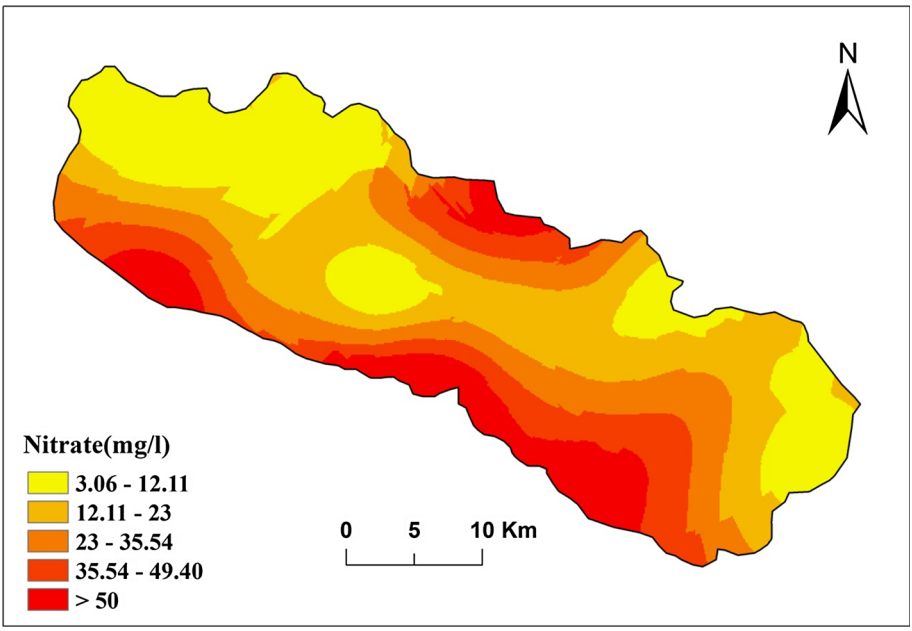

Fig. 4 Spatial distribution of nitrate concentration over the study area

$$\sum_{A \subset \Theta} m(A) = 1$$

This finding implies that no Bel should be fixed to an empty set and that the total Bel should amount to one. The Bel and Pls functions are defined according to the mass function. Equation (4) represents Bel, which is committed to a proposition H, as follows:

$$\mathrm{Bel}(H) = \sum_{A \subset H} m(A). \tag{4}$$

The possible maximum Bel level is denoted by the Pls, but can also represent the maximum level to which the hypothesis cannot be disbelieved, provided that sufficient evidence that contradicts the hypotheses is available. The bpas relevant to the subsets of the hypothesis (H) complement is subtracted to acquire the Pls (Gorsevski et al. 2005). The sum of the probability masses assigned to all sets with non-empty intersections to the propositions is equivalent to the Pls (Baraldi and Zio 2010). The following expression defines the Pls function (Gorsevski et al. 2005):

$$\mathrm{Pls}(H) = \sum_{A \cap H \neq \emptyset} m(A). \tag{5}$$

The Pls and Bel functions are the upper and lower boundaries, respectively, of the class of probability assignments on H that expresses the following characteristics;

$$\mathrm{Bel}(H) \leq \mathrm{Pls}\ (H), \tag{6}$$

$$\mathrm{Pls}(H) = 1 - \mathrm{Bel}(H^{-}),$$

where the negation of H is denoted by H^{-}, whereas the disbelief function (Dis) is denoted by Bel (H^{-}). The belief of the proposition is denoted by Dis, which is false on the given evidence and expressed as follows:

$$\mathrm{Dis} = 1 - \mathrm{Pls\ or}\ 1 - \mathrm{Unc} - \mathrm{Bel}. \tag{7}$$

Equation (8) provides the degree of uncertainty (Unc) regarding H:

$$\mathrm{Unc}(H) = \mathrm{Pls}(H) - \mathrm{Bel}(H). \tag{8}$$

The difference between Bel and Pls is expressed as Unc, which is quantified as the amount of evidence that is not assigned to any specific subset when the degree of uncertainty is zero (An et al. 1992). Pieces of evidence related to individual hypothesis were collected by DST. Carranza and Hale (2002) and Carranza et al. (2008) explained that

$$\mathrm{Bel} + \mathrm{Unc} + \mathrm{Dis} = 1. \tag{9}$$

4.4 Combining data by using DST

DST has been identified among the emerging spatial data integration models based on the evidence provided by Shafer (1976). A mathematical framework is provided by DST to represent and combine information.

A frame of discernment can be specified according to DST of evidence, as follows:

$$m : 2^{\Theta} \rightarrow [T_p, \Theta, \emptyset, T_p^-]. \tag{10}$$

The target proposition is denoted by T_p, provided that nitrate ≥50 mg/L is at each pixel p, whereas T_p^- denotes an opposite target proposition, such that nitrate ≥50 mg/L is not involved at each pixel p.

Information is combined with mathematical theory of evidence by applying Dempster's rule. Two mass functions are represented by m_1 and m_2, respectively, whereas Dempster's rule of combination defines the combined mass function.

$$m(H) = m1 \oplus m2 = \frac{\sum_{Ai \cap Bj} m_1(A_i).m_2(B_j)}{1-k}, \tag{11}$$

where $k = \sum_{Ai \cap Bj} m_1(A_i).m_2(B_j) < 1$.

The basic mass probability related to conflict is represented by k. The products of the *bpas* of all sets are summed up to fulfill this objective, provided that the intersection is null. This rule is not continuous, but commutative and associative.

The normalization factor is given by the denominator in Dempster's rule, $1-k$.

The total probability is defined by the constant k in Eq. (11), which is associated with the disjoint subsets of H. A measure of conflict between two pieces of evidence is provided by this constant. Two pieces of evidence contradict each other when $k = 1$, but their basic probability cannot be orthogonally summed up.

An area subjected to groundwater pollution study may contain seven multiple spatial layers of DRASTIC. Each layer is regarded as evidence E_i $(i = D, R, A, S, T, I, C)$ for the target proposition T_p. The probability ratio $\lambda(T_p)E_{ij}$ to support the positive target proposition is defined by Eq. (12) when E_{ij} is provided. E_{ij} denotes the jth class attribute of evidence E_i in the presence of the frequency distribution functions of the positive and opposite target propositions.

$$\lambda(Tp)Eij = \frac{\frac{N(L \cap E_{ij})}{N(L)}}{\frac{N(E_{ij}) - N(L \cap E_{ij})}{N(A) - N(L)}} \tag{12}$$

The number of nitrate occurrence pixels is denoted by $N(L \cap E_{ij})$ within the range, and greater than 50 mg/L is obtained in E_{ij}. The total number of all nitrate occurrence pixels is denoted by $N(L)$, which lies within the range of ≥50 mg/L. The number of pixels in E_{ij} is given by $N(E_{ij})$, and the number of pixels in the entire study area A is denoted by $N(A)$. The proportion of nitrate occurrence in the given attribute E_{ij} is denoted by the numerator, whereas the proportion of nitrate <50 mg/L areas in the given attribute E_{ij} is presented by the denominator. The value of the likelihood ratio may vary from 0 to infinity. The following expression defines the probability ratio to support the opposite target proposition:

$$\lambda\left(T_p^-\right)E_{ij} = \frac{\frac{N(L) - N(L \cap E_{ij})}{N(L)}}{\frac{N(A) - N(L) - N(E_{ij}) + N(L \cap E_{ij})}{N(A) - N(L)}}. \tag{13}$$

The mass function can be derived through the standardization procedure applied on the two likelihood ratio functions. The sum of the likelihood ratio values of all class attributes in the given evidence E_i is used to divide the likelihood ratios. This step also estimates relative importance within class attribute values while applying standard conditions in Eq. (3):

$$m(T_p)E_{ij} = \frac{\lambda(T_p)E_{ij}}{\sum_j \lambda(T_p)E_{ij}}, \tag{14}$$

$$m\left(T_p^-\right)E_{ij} = \frac{\left(T_p^-\right)E_{ij}}{\sum_j \left(T_p^-\right)E_{ij}},$$

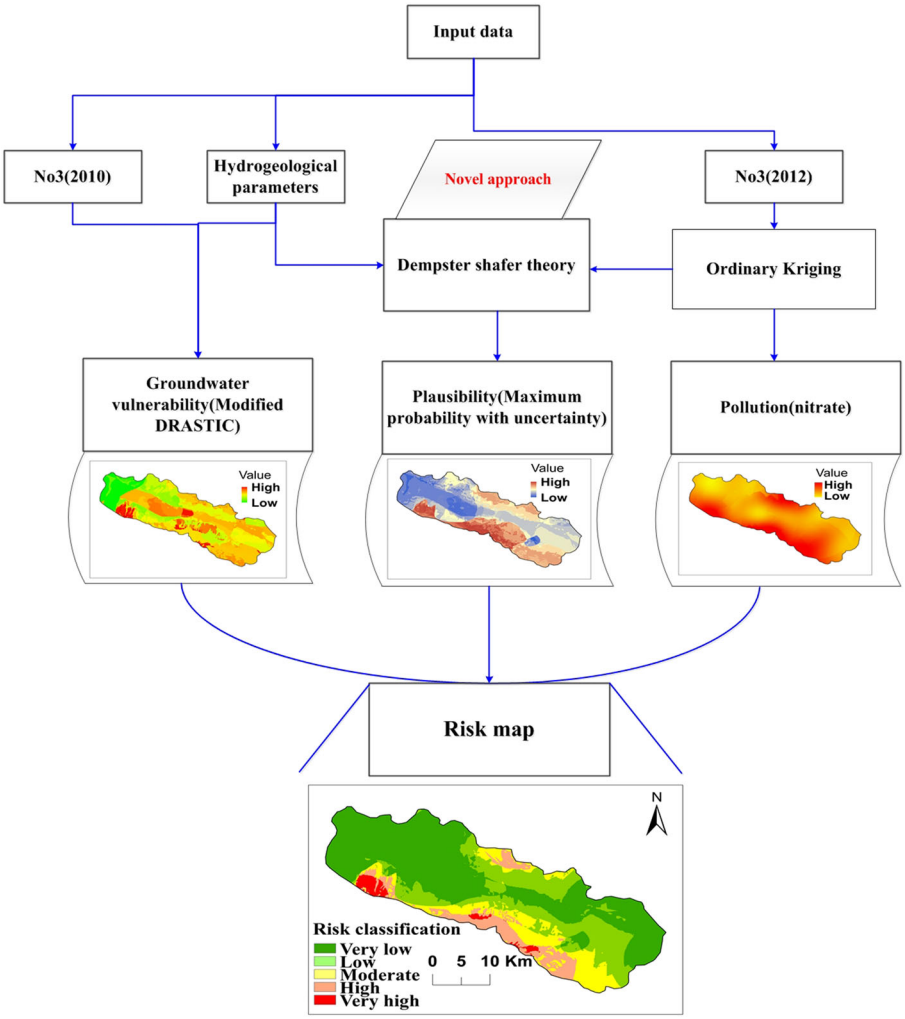

Fig. 5 Overall methodology used in the study

$$m(\Theta)E_{ij} = 1 - m(T_p)E_{ij} - m\left(T_p^-\right)E_{ij}.$$

The belief function of the positive target proposition can be directly extracted from the mass function $m(Tp)Eij$ by considering the frame of discernment in Eq. (10). Equation (15) can evaluate the Pls function, as follows:

$$\text{Pls} = 1 - m\left(T_p^-\right)E_{ij}. \tag{15}$$

Figure 5 depicts the overall methodology used in this study.

5 Results and discussion

The groundwater risk assessment depended on three factors: groundwater vulnerability; pollution; and the probability of pollution occurrence.

$$\text{Risk} = \text{Vulnerability} \times \text{Pollution} \times \text{Pollution Occurrence Probability}$$

The modified DRASTIC map provided more reliable result with the highest accuracy compared with the original DRASTIC model and other modification methods applied in the study area. In addition, kriging interpolation was used to produce a continuous map of the spatial distribution of nitrate concentration based on the weighted average of the measured sample locations. DST was applied, and the probability of pollution occurrence in the area with considering uncertainty was also identified.

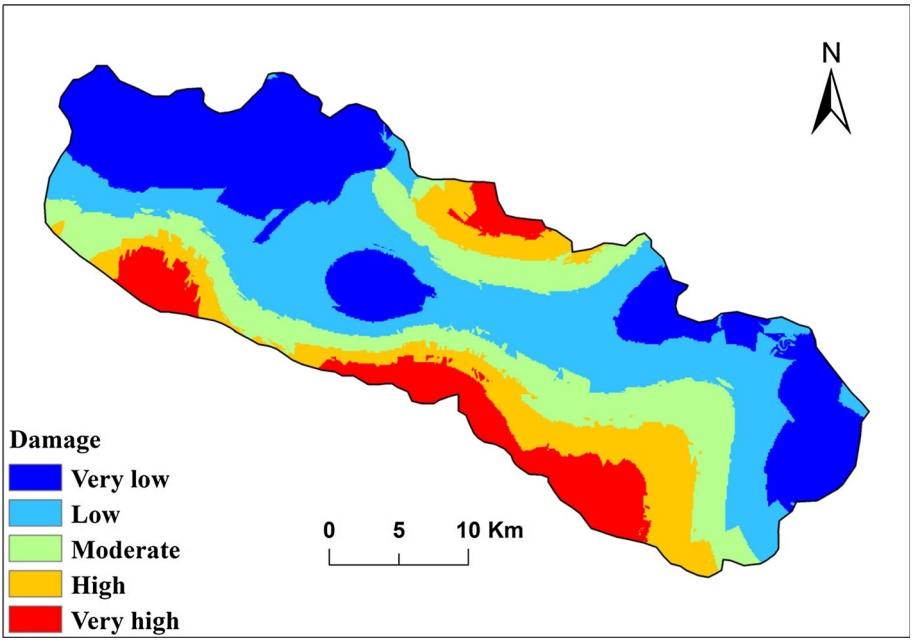

Fig. 6 Damage index map

Table 1 Values of DST for classes of DRASTIC parameters

Parameter	Range	Number of class pixel	Number of nitrate pixels ≥ 50	Belief	Disbelief	Uncertainty	Plausibility
Depth of water(m)	15–23	9739	0.00	0.00	0.45	0.55	0.55
	23–30	53,976	1710	0.22	0.45	0.33	0.55
	>30	4,299,424	455,616	0.78	0.10	0.11	0.90
Net recharge (mm)	0–50.8	769,651	8117	0.04	0.41	0.55	0.59
	50.8–101.6	1,946,202	197,401	0.37	0.35	0.28	0.65
	101.6–177.8	1,647,349	251,809	0.59	0.24	0.17	0.76
Aquifer media	Marlstone	280,921	100,800	0.73	0.17	0.10	0.83
	Sandstone	8213	595	0.10	0.21	0.69	079
	Fine medium sand	682,918	0.00	0.00	0.25	0.75	0.75
	Silt and clay	295,422	0.00	0.00	0.22	0.78	0.78
	Gravel sand	3,095,728	355,931	0.17	0.15	0.68	0.85
Soil media			56,748	0.70	0.13	017	0.87
	Gravel	110,911	0.00	0.00	0.18	0.82	0.82
	Silty loam	746,310	0.00	0.00	0.18	0.82	0.82
	Clay loam	739,032	6337	0.00	0.18	0.82	0.82
	Loam	867,112	392,764	0.29	0.03	0.68	0.97
	Sand	1,292,821	0.00	0.00	0.16	0.84	0.84
	Non-shrinking	337,955	1477	0.00	0.15	0.84	0.85
	Sandy loam	269,090					
Topography (slope %)	0–2	1,003,466	2084	0.00	0.26	0.73	0.74
	2–6	1,462,183	63,732	0.05	0.26	0.69	0.74
	6–12	1,432,714	276,128	0.24	0.11	0.65	0.89
	12–18	340,736	80,202	0.31	0.17	0.51	0.83
	>18	124,255	34,972	0.40	0.19	0.42	0.81
Vadose zone impact	Marlstone Shale	277,285	100,740	0.67	0.17	0.16	0.83
	Sand Gravel	557,511	7929	0.02	0.24	0.75	0.77
	Conglomerate	9094	1082	0.16	0.21	0.64	0.80
	Sand Gravel w Silt	2,994,564	347,575	0.15	0.15	0.69	0.84
	Silt/Clay	524,748	0.00	0.00	0.24	0.76	0.76
Hydraulic conductivity (m/day)	< 4	769,651	251,809	0.81	0.16	0.03	0.84
	4–12	1,551,690	8117	0.01	0.50	0.49	0.50
	12–28	2,041,790	197,401	0.18	0.33	0.49	0.67

5.1 Damage map

Damage must be identified and quantified to obtain a groundwater pollution risk map. The study area is primarily associated with agricultural activities, and thus assessment should focused on the threats from these activities. The nitrate concentration map derived from interpolation of nitrate concentration was multiplied by the modified DRASTIC map in the study area to obtain the damage map (Fig. 6).It is can be described as follow;

$$\text{Damage} = \text{Vulnerability} \times \text{Pollution}$$

Five categories were used for the damage index. The southern region and a small section of the northern region exhibited the highest damage index. Therefore, these areas should be focused on during risk assessment.

5.2 Applying DST to groundwater pollution risk assessment

The results are represented by DST through a range of probabilities by using natural variability and model uncertainty (Sentz and Ferson, 2002; Helton 2008). Spatial integration of the damage map and the probability occurrence of pollution by using DST were conducted to obtain the basic groundwater pollution risk map. Afterward, the results were reclassified.

The sum of the lower probability and uncertainty occurrence leads to the highest probability of pollution occurrence. In the DRASTIC parameters (Table 1), the depth of water within the range of >30 m exhibited the highest Bel and low Unc values, thus indicating the highest probability of pollution occurrence. Therefore, aggregating probabilities by considering the uncertainty was indicated as Pls, which was used in risk assessment. Meanwhile, the recharge parameter within the range of 101.6–177.8 mm exhibited high Bel value and the lowest uncertainty value, thus indicating the highest probability of pollution occurrence.

Marlstone–shale and gravel–sand indicated the highest Pls value for the aquifer media. The former showed high Bel and low Unc values, whereas the latter presented low Bel and high Unc values. Based on the interpretation of the Bel values for the soil type parameter, gravel presents a high probability of groundwater pollution occurrence. However, sand has the highest probability because of the sum of the Bel and the Unc values. The Bel values for the remaining categories are relatively low and indicate a low probability of groundwater pollution. In the case of the topography parameter, slope angles with values more than 18 % have a high Bel, thus indicating the highest probability of pollution, followed by slope angles ranging from 12 to 18 %, and then those from 6 to 12 %. For the impact of the vadose zone parameter, marlstone–shale exhibits the highest possibility of nitrate pollution occurrence, thus suggesting a higher probability of pollution occurrence than other vadose zone types.

Dempster's combination rule was applied to investigate additional information sources to simulate the process of forming a Bel function regarding groundwater pollution occurrences. The combination results indicated that nitrate ≥50 mg/L observations are the most appropriate indicators of pollution occurrences. Eqs in (12)–(15) consider the spatial relationship of an evidential data layer with a nitrate concentration ≥50 mg/L and the relationship between the subsets of each DRASTIC parameter within an evidential data layer.

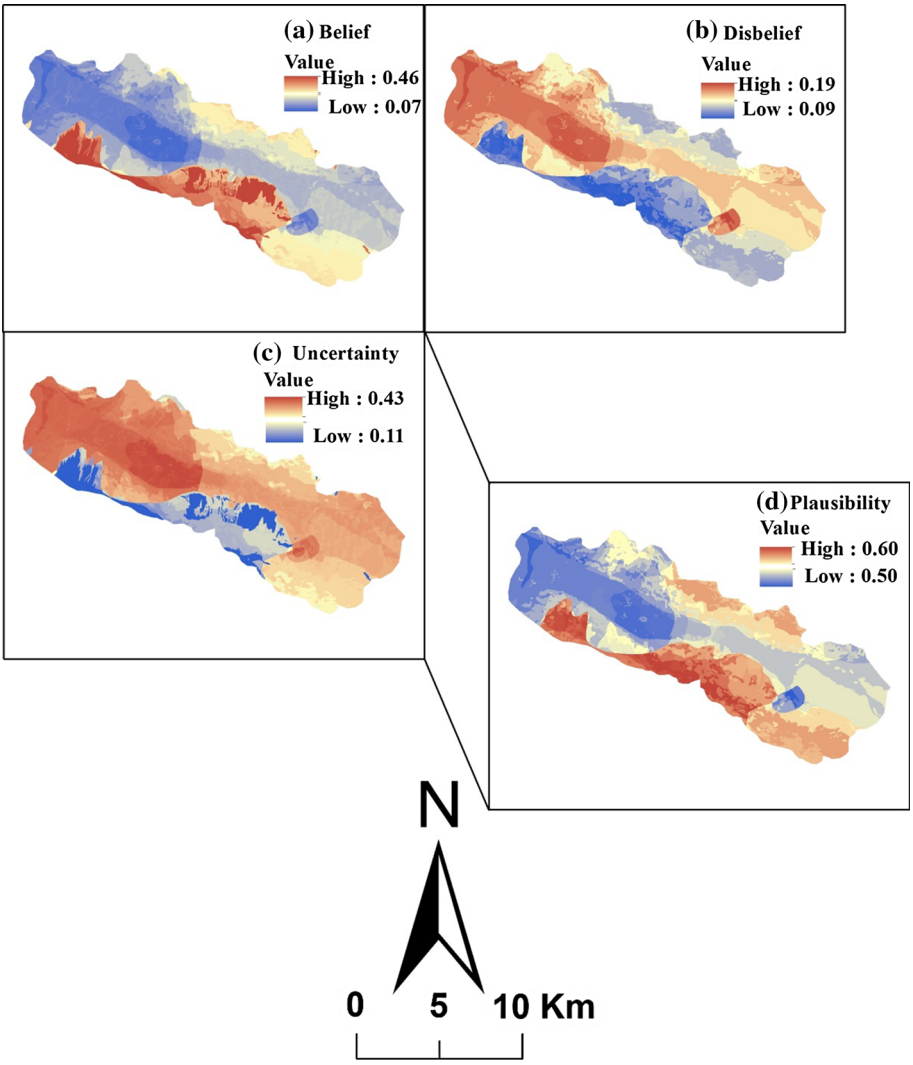

Fig. 7 Integration results derived from DST

The integrated results derived from DST are shown in Fig. 7. The Bel values in areas with low disbelief values are high, as shown in the comparison between the Bel map and the Dis map. Areas with a high degree of Bel and a low degree of Dis for pollution occurrence are vulnerable to groundwater pollution. Information that supports uncertainty of pollution occurrence was missing from the uncertainty map. The difference between Pls and Bel functions is called uncertainty. Areas with low Bel values exhibit high uncertainty values. Areas with high Bel and uncertainty values also present high values in the Pls map.

5.2.1 Risk mapping

In this research, the groundwater pollution risk map was deduced mainly from the combination of the damage and the probability occurrence of pollution that considers uncertainty. The DST approach was used to conduct evaluation probability with regard to uncertainty. Probability-based evaluation was successfully used to characterize the uncertainties of the parameters. The value of risk and pollution resulting from the presence of nitrates in groundwater was estimated as ≥50 mg/L. The integrated map of the degrees of plausibility produced cautionary information that represents potentially polluted areas (information that provides support for the proposition that nitrate ≥50 mg/L is sufficient) and the areas that require spatial evidence (information on spatial evidence that provides support for the proposition that nitrate ≥50 mg/L is insufficient). Therefore, the aforementioned map was applied to multiply the damage map and produce the final risk map.

Combining the damage and probability maps, it is used to produce the groundwater pollution risk map of the Kerman Plain. Equation (16) indicates that the damage is denoted by *Di*, and the probability of occurrence is denoted by *Pi*:

$$\text{Risk} = \sum_{i=1}^{R} P_i \times D_i. \tag{16}$$

The risk map and the percentages of each class in the study area is illustrated in Figs. 8 and 9, respectively. The very low and low risk areas cover 75 % of the entire plain, which comprises the northeast, northwest, and central parts of the study area, thus indicating good correspondence of the spatial distribution of nitrate concentration. Moderate pollution risk

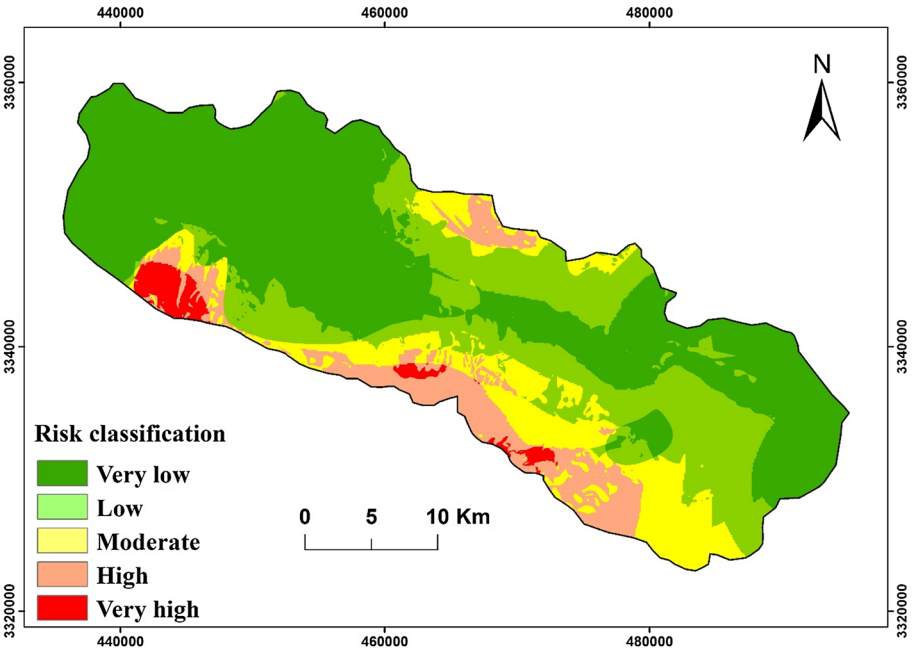

Fig. 8 Risk map classification

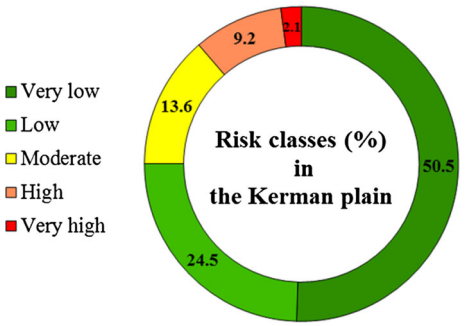

Fig. 9 Risk percentages for each class

(13.6 % of the plain) for groundwater is also depicted in regions close to the high- and very high risk zones in the study area. The high- and very high risk areas cover approximately 11.3 % of the plain and comprise the southern part, particularly, the southeast and southwest portions, and a small section of the northern part. Groundwater resources with high permeability located in the northern and southern regions of the study area under a permeable surface consist of gravel and sand. Marlstone–shale formations and higher slope ranges are other indicators that are relevant to a high risk level.

6 Conclusion

Spatial analysis of groundwater pollution is relevant to agricultural activities, which requires robust methods. This study introduced a new way to assess groundwater pollution risk and design a monitoring system for future. It combined groundwater vulnerability, pollution, and probability with respect to uncertainty within a new framework. We attempted to represent how the probability measurement with incomplete information in the role of uncertainty can be used by environmental resource managers. The outcomes indicated that the development of risk assessment based on probability and uncertainty was possible.

The probability and uncertainty for a spatial distribution of polluted areas that exceed a threshold value were provided through DST technique in the Kerman plain. Characterization of the uncertainties of parameter classifications and ratings is understood through this framework, thus providing a new perspective into this aspect.

Identification of groundwater pollution risk due to applying of fertilizers demonstrates the areas in which we would focus efforts to reduce risk by using advanced techniques of fertilization in agricultural lands. Risk map optimizes the qualitative monitoring system. The maps indicate five priority zones diagnosed for the construction of a monitoring system. Moreover, high-risk zones that exhibited an increase may enhance monitoring.

Applying this methodology is recommended by the authors if the objective is to develop a risk map of areas that are vulnerable to pollution. Furthermore, aside from nitrate, other pollutants can also be identified in other regions, thus urging analysts to search for other factors that lead to pollution of groundwater resources.

References

Aller L, Bennet T, Lehr JH, Petty RJ, Hackett G (1987) DRASTIC: a standardized system for evaluating groundwater pollution potential using hydrogeological settings

An P, Moon WM, Bonham-Carter GF (1992) On knowledge-based approach of integrating remote sensing, geophysical and geological information. In: Geoscience and Remote Sensing Symposium, pp 34–38

Anane M, Bouziri L, Limam A, Jellali S (2012) Ranking suitable sites for irrigation with reclaimed water in the Nabeul-Hammamet region (Tunisia) using GIS and AHP-multicriteria decision analysis. Resour Conserv Recy 65:36–46

Antonakos AK, Lambrakis NJ (2007) Development and testing of three hybrid methods for the assessment of aquifer vulnerability to nitrates, based on the drastic model, an example from NE Korinthia, Greece. J Hydrol 333:288–304. doi:10.1016/j.jhydrol.2006.08.014

Assaf H, Saadeh M (2009) Geostatistical assessment of groundwater nitrate contamination with reflection on DRASTIC vulnerability assessment: the case of the upper litani basin, Lebanon. Water Resour Manage 23:775–796. doi:10.1007/s11269-008-9299-8

Baalousha H (2010) Assessment of a groundwater quality monitoring network using vulnerability mapping and geostatistics: a case study from Heretaunga Plains, New Zealand. Agric Water Manage 97:240–246. doi:10.1016/j.agwat.2009.09.013

Babiker IS, Mohamed MAA, Hiyama T, Kato K (2005) A GIS-based DRASTIC model for assessing aquifer vulnerability in Kakamigahara Heights, Gifu Prefecture, Central Japan. Sci Total Environ 345:127–140. doi:10.1016/j.scitotenv.2004.11.005

Baraldi P, Zio E (2010) A comparison between probabilistic and dempster-shafer theory approaches to model uncertainty analysis in the performance assessment of radioactive waste repositories. Risk Anal 30:1139–1156. doi:10.1111/j.1539-6924.2010.01416.x

Bayat B, Nasseri M, Zahraie B (2014) Identification of long-term annual pattern of meteorological drought based on spatiotemporal methods: evaluation of different geostatistical approaches. Nat Hazards 76:515–541. doi:10.1007/s11069-014-1499-3

Carranza EJM (2011) Analysis and mapping of geochemical anomalies using logratio-transformed stream sediment data with censored values. J Geochem Explor 110:167–185. doi:10.1016/j.gexplo.2011.05.007

Carranza EJM, Castro OT (2006) Predicting Lahar-Inundation Zones: case study in West Mount Pinatubo, Philippines. Nat Hazards 37:331–372. doi:10.1007/s11069-005-6141-y

Carranza EJM, Hale M (2002) Spatial association of mineral occurrences and curvilinear geological features. Math Geo l34: 203–221

Carranza EJM, Sadeghi M (2010) Predictive mapping of prospectivity and quantitative estimation of undiscovered VMS deposits in Skellefte district (Sweden). Ore Geol Rev 38:219–241. doi:10.1016/j.oregeorev.2010.02.003

Carranza EJM, Hale M, Faassen C (2008) Selection of coherent deposit-type locations and their application in data-driven mineral prospectivity mapping. Ore Geol Rev 33:536–558. doi:10.1016/j.oregeorev.2007.07.001

Cayuela L, Golicher JD, Rey JS, Benayas JMR (2006) Classification of a complex landscape using Dempster-Shafer theory of evidence. Int J Remote Sens 27:1951–1971. doi:10.1080/01431160500181788

Chen SK, Jang CS, Peng YH (2013) Developing a probability-based model of aquifer vulnerability in an agricultural region. J Hydrol 486:494–504. doi:10.1016/j.jhydrol.2013.02.019

Chica-Olmo M, Luque-Espinar JA, Rodriguez-Galiano V, Pardo-Igúzquiza E, Chica-Rivas L (2014) Categorical Indicator Kriging for assessing the risk of groundwater nitrate pollution: the case of Vega de Granada aquifer (SE Spain). Sci Total Environ 470–471:229–239. doi:10.1016/j.scitotenv.2013.09.077

Chowdhury S, Champagne P, McLellan PJ (2009) Uncertainty characterization approaches for risk assessment of DBPs in drinking water: a review. J Environ Manag 90:1680–1691. doi:10.1016/j.jenvman.2008.12.014

Cucchi F, Franceschini G, Zini L, Aurighi M (2008) Intrinsic vulnerability assessment of Sette Comuni Plateau aquifer (Veneto Region, Italy). J Environ Manage 88:984–994. doi:10.1016/j.jenvman.2007.05.007

Dempster AP (1967) Upper and lower probabilities induced by a multivalued mapping. Ann Math Stat 38:325–339

Dimitriou E, Karaouzas I, Sarantakos K, Zacharias I, Bogdanos K, Diapoulis A (2008) Groundwater risk assessment at a heavily industrialised catchment and the associated impacts on a peri-urban wetland. J Environ Manag 88:526–538. doi:10.1016/j.jenvman.2007.03.019

Feizizadeh B, Blaschke T (2012) GIS-multicriteria decision analysis for landslide susceptibility mapping: comparing three methods for the Urmia lake basin, Iran. Nat Hazards 65:2105–2128. doi:10.1007/s11069-012-0463-3

Fijani E, Nadiri AA, Asghari Moghaddam A, Tsai FTC, Dixon B (2013) Optimization of DRASTIC method by supervised committee machine artificial intelligence to assess groundwater vulnerability for Maragheh-Bonab plain aquifer, Iran. J Hydrol 503:89–100. doi:10.1016/j.jhydrol.2013.08.038

Ghosh S, Carranza EJM (2010) Spatial analysis of mutual fault/fracture and slope controls on rocksliding in Darjeeling Himalaya, India. Geomorphology 122:1–24. doi:10.1016/j.geomorph.2010.05.008

Gorsevski PV, Jankowski P, Gessler PE (2005) Spatial prediction of landslide hazard using Fuzzy k-means and Dempster–Shafer theory. Trans GIS 9:455–474. doi:10.1111/j.1467-9671.2005.00229.x

Helton JC (2008) Uncertainty and sensitivity analysis for models of complex systems computational methods in transport: verification and validation. Springer, Heidelberg, pp 207–228. doi:10.1007/978-3-540-77362-7_9

Javadi S, Kavehkar N, Mohammadi K, Khodadadi A, Kahawita R (2011) Calibrating DRASTIC using field measurements, sensitivity analysis and statistical methods to assess groundwater vulnerability. Water Int 36:719–732. doi:10.1080/02508060.2011.610921

Jebur MN, Pradhan B, Tehrany MS (2015) Manifestation of LiDAR-derived parameters in the spatial prediction of landslides using novel ensemble evidential belief functions and support vector machine models in GIS. IEEE J Sel Top Appl 8:674–690. doi:10.1109/jstars.2014.2341276

Leone A, Ripa MN, Uricchio V, Deák J, Vargay Z (2009) Vulnerability and risk evaluation of agricultural nitrogen pollution for Hungary's main aquifer using DRASTIC and GLEAMS models. J Environ Manage 90:2969–2978. doi:10.1016/j.jenvman.2007.08.009

Malpica JA, Alonso MC, Sanz MA (2007) Dempster-Shafer theory in geographic information systems, a survey. Expert Syst Appl 32:47–55

Manos B, Papathanasiou J, Bournaris T, Voudouris K (2010) A multicriteria model for planning agricultural regions within a context of groundwater rational management. J Environ Manag 91:1593–1600

Mishra U, Lal R, Liu D, Van Meirvenne M (2010) Predicting the spatial variation of the soil organic carbon pool at a regional scale. Soil Sci Soc Am J 74:906. doi:10.2136/sssaj2009.0158

Mohammady M, Pourghasemi HR, Pradhan B (2012) Landslide susceptibility mapping at Golestan Province, Iran: a comparison between frequency ratio, Dempster-Shafer, and weights-of-evidence models. J Asian Earth Sci 61:221–236

Moon WM (1990) Integration of geophysical and geological data using evidential belief function. IEEE T Geosci Remote 28:711–720

Nampak H, Pradhan B, Manap MA (2014) Application of GIS based data driven evidential belief function model to predict groundwater potential zonation. J Hydrol 513:283–300. doi:10.1016/j.jhydrol.2014.02.053

Napolitano P, Fabbri AG (1996) Single-parameter sensitivity analysis for aquifer vulnerability assessment using DRASTIC and SINTACS. In: IAHS publications-series of proceedings and reports-intern Association Hydrological Sciences 235: 559–566

Neshat A, Pradhan B (2014) An integrated DRASTIC model using frequency ratio and two new hybrid methods for groundwater vulnerability assessment. Nat Hazards 76:543–563. doi:10.1007/s11069-014-1503-y

Neshat A, Pradhan B, Pirasteh S, Shafri HZM (2013) Estimating groundwater vulnerability to pollution using a modified DRASTIC model in the Kerman agricultural area, Iran. Environ Earth Sci 71:3119–3131. doi:10.1007/s12665-013-2690-7

Neshat A, Pradhan B, Dadras M (2014) Groundwater vulnerability assessment using an improved DRASTIC method in GIS. Resour Conserv Recy 86:74–86. doi:10.1016/j.resconrec.2014.02.008

Neshat A, Pradhan B, Javadi S (2015) Risk assessment of groundwater pollution using Monte Carlo approach in an agricultural region: an example from Kerman Plain, Iran. Comput Environ Urban Syst 50:66–73. doi:10.1016/j.compenvurbsys.2014.11.004

Pacheco FAL, Sanches Fernandes LF (2013) The multivariate statistical structure of DRASTIC model. J Hydrol 476:442–459. doi:10.1016/j.jhydrol.2012.11.020

Pavlis M, Cummins E (2014) Assessing the vulnerability of groundwater to pollution in Ireland based on the COST-620 Pan-European approach. J Environ Manag 133:162–173. doi:10.1016/j.jenvman.2013.11.044

Pradhan B, Abokharima MH, Jebur MN, Tehrany MS (2014) Land subsidence susceptibility mapping at Kinta Valley (Malaysia) using the evidential belief function model in GIS. Nat Hazards 73:1019–1042. doi:10.1007/s11069-014-1128-1

Saidi S, Bouri S, Ben Dhia H, Anselme B (2011) Assessment of groundwater risk using intrinsic vulnerability and hazard mapping: application to Souassi aquifer, Tunisian Sahel. Agric Water Manag 98:1671–1682. doi:10.1016/j.agwat.2011.06.005

Sentz K, Ferson S (2002) Combination of Evidence in Dempster-Shafer Theory. doi:10.2172/800792

Shafer G (1976) A mathematical theory of evidence. Princeton University Press, Princeton

Sorichetta A, Masetti M, Ballabio C, Sterlacchini S, Beretta GP (2011) Reliability of groundwater vulnerability maps obtained through statistical methods. J Environ Manag 92:1215–1224. doi:10.1016/j.jenvman.2010.12.009

Stigter TY, Ribeiro L, Carvalho Dill AMM (2006) Application of a groundwater quality index as an assessment and communication tool in agro-environmental policies—two Portuguese case studies. J Hydrol 327:578–591. doi:10.1016/j.jhydrol.2005.12.001

Tesoriero AJ, Duff JH, Wolock DM, Spahr NE, Almendinger JE (2009) Identifying pathways and processes affecting nitrate and orthophosphate inputs to streams in agricultural watersheds. J Environ Qual 38:1892–1900. doi:10.2134/jeq2008.0484

Thiam AK (2005) An evidential reasoning approach to land degradation evaluation: dempster-shafer theory of evidence. Trans GIS 9:507–520. doi:10.1111/j.1467-9671.2005.00232.x

Tien Bui D, Pradhan B, Lofman O, Revhaug I, Dick OB (2012) Spatial prediction of landslide hazards in Hoa Binh province (Vietnam): a comparative assessment of the efficacy of evidential belief functions and fuzzy logic models. CATENA 96:28–40. doi:10.1016/j.catena.2012.04.001

Tien Bui D, Pradhan B, Lofman O, Revhaug I, Dick OB (2013) Regional prediction of landslide hazard using probability analysis of intense rainfall in the Hoa Binh Province, Vietnam. Nat Hazards 66(2):707–730. doi:10.1007/s11069-012-0510-0

Van Beynen PE, Niedzielski MA, Bialkowska-Jelinska E, Alsharif K, Matusick J (2012) Comparative study of specific groundwater vulnerability of a karst aquifer in central Florida. Appl Geogr 32:868–877. doi:10.1016/j.apgeog.2011.09.005

Wang J, He J, Chen H (2012) Assessment of groundwater contamination risk using hazard quantification, a modified DRASTIC model and groundwater value, Beijing Plain, China. Sci Total Environ 432:216–226. doi:10.1016/j.scitotenv.2012.06.005

Wang K, Zhang C, Li W (2013) Predictive mapping of soil total nitrogen at a regional scale: a comparison between geographically weighted regression and cokriging. Appl Geogr 42:73–85. doi:10.1016/j.apgeog.2013.04.002

Wilcoxon F (1945) Individual comparisons by ranking methods. Biometrics 1:80–83